Optics Letters

Geometric phase in distributed fiber optic sensing

SABAHAT SHAHEEN* AND KONSTANTIN HICKE

The Federal Institute for Materials Research and Testing, Unter den Eichen 87, 12205, Berlin, Germany
**Corresponding author: sabahat.shaheen@bam.de*

Received 19 May 2022; revised 7 July 2022; accepted 8 July 2022; posted 11 July 2022; published 28 July 2022

The geometric phase in the beat signal from coherent interference of two frequency-offset light beams is measured using a novel distributed optical fiber sensing setup. In a fiber optic medium, with changing beam intensities, to the best of our knowledge, ours is the first measurement of the mentioned geometric phase. Experimental results of applying a 100-Hz sinusoidal stimulus to a polarization scrambler and a piezoelectric transducer inline to an optical fiber are presented. The results may enable novel distributed fiber sensing techniques.

https://doi.org/10.1364/OL.464259

Introduction. When the polarization state of light traverses a path on the Poincaré sphere, it acquires a geometric phase in direct proportion to half the solid angle subtended at the center of the sphere by the path traversed [1]. This may happen in the spatial domain when light itself traverses a circular path, for example, when light travels through a helically wound optical fiber [2] or through a quarter- or half-wave plate [3]. The geometric phase and its manipulation may be used in opto-electronics setups as a design parameter [3]. Especially relevant to our work is the use of the geometric phase to design optical fiber distributed sensors [4–6]. The geometric phase may also exist in the time domain, i.e., without rotating the path of light, as long as its state-of-polarization (SOP) undergoes rotation; as was recently theorized and demonstrated in a double pinhole experiment [7], in two-beam interference [8], as well as in interference between two frequency-offset beams [9]. We focus on the latter case where the phase of the beat signal of two frequency-offset beams acquires a periodically varying geometric component, as long as the two beams have different SOPs [9]. When this condition is true, the SOP of the resultant beat signal traverses a complete circle on the Poincaré sphere in each beat period, thus giving rise to a geometric phase in the time domain. This phase is a function of the relative intensity and SOP, respectively, of the two interfering beams. Moreover, the total phase of light with angular velocity, ω, in each beat period, T, remains constant, equal to $\omega T \pm \pi$, divided into the geometric and the remaining dynamic components [9].

The coupling between the geometric and the dynamic phases motivates one to measure the geometric phase in a distributed fiber sensing setup, where the dynamic phase is used as a measurand [10], and evaluate its utility as an alternative to or to augment the information obtained from the dynamic phase. This is in turn motivated by the fact that the condition for the existence of the geometric phase is complimentary to that of the dynamic phase. Dynamic phase measurement using coherent heterodyne detection assumes that the state-of-polarization of the two beams is identical [11,12], whereas for the existence of the geometric phase, they must not be so [9]. In fact, the condition of identical SOPs of the two beams becomes a challenge for measuring the dynamic phase, given that the polarization of light in an optical fiber does not necessarily remain constant beyond a few meters [11–13]. Given these considerations, it is anticipated that a sensing mechanism based on the geometric phase will be free from polarization-mismatch fading. Phase-sensitive optical time-domain reflectometry, ϕ-OTDR, is one of the current state-of-the-art technologies for distributed fiber sensing [14]. It is currently being investigated for better performance in terms of higher dynamic range, spatial resolution, and other respects, for applications in seismic sensing, structural health, and infrastructure monitoring, among others [10,14]. Coherent heterodyne detection [11] is one of the methods used in ϕ-OTDR for demodulation of the dynamic phase [12]. In fact, ϕ-OTDR based on coherent heterodyne detection [12] provides a context in which the geometric phase may exist, i.e., coherent interference of light beams with a frequency offset, subject to the condition that the SOPs of the interfering beams are not exactly the same [9]. We note that the original work on the measurement of the geometric phase in the beating of light waves is done using free-space optics with beams of constant intensity [9].

In this work, we measure the geometric phase in the optical fiber medium to use it in distributed fiber optic sensing [10], such that one of the interfering beams has changing intensity (i.e., backscattered signal) while the other is the constant-intensity local oscillator (LO) signal [10]. In this Letter, we first analyze the expression [9] for calculating the geometric phase, followed by a description of our experimental setup designed for its measurement. Two cases of stimulation of a fiber-under-test by an acoustic signal, applied to a polarization scrambler and a piezoelectric transducer, are presented and discussed.

Theory and experimental setup. The expression for the geometric phase, ϕ_g, is given as [9]

$$\phi_g = \pm\pi - \sum_{n=1}^{N} arg[S_0' exp(\frac{-i\pi}{N}) + S_0'' exp(\frac{i\pi}{N}) + 2\sqrt{S_0' S_0''}|\gamma_0| cos(\frac{n2\pi}{N})], \quad (1)$$

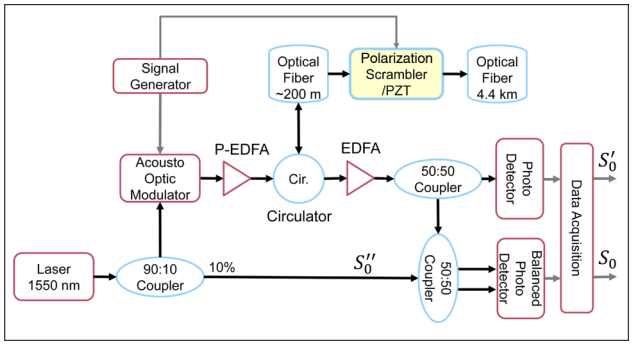

Fig. 1. Experimental setup of the proposed ϕ-OTDR used to measure the geometric phase, ϕ_g. PZT, piezoelectric transducer; P-EDFA, pulsed erbium-doped fiber amplifier; EDFA, erbium-doped fiber amplifier.

where S_0 is the beat signal obtained from coherent heterodyning of two beams with intensities S_0' and S_0'', and ϕ_g is calculated over a beat period that is divided into N integer number of sections. The sign of π in Eq. (1) is chosen to conform to the condition $\phi \leq \pi$. It is noted that the positive or negative sign of the geometric phase corresponds to clockwise or counterclockwise motion of the SOP around the Poincaré sphere [9]. Here, $|\gamma_0|$ is the normalized amplitude of the beat signal given by [9]

$$\gamma_0 = S_0/\sqrt{S_0' S_0''}. \tag{2}$$

Equation (1) shows that to calculate ϕ_g, we require individual beam intensities, S_0', S_0'', and the normalized beat signal, γ_0[9]. The envelope signal, $|\gamma_0|$, is extracted by taking the Hilbert transform of the beat signal, S_0, after normalizing it as per Eq. (2). Our proposed setup to calculate the geometric phase is based on standard coherent heterodyne ϕ-OTDR, which also relies on S_0 to extract the dynamic phase [12]. The difference from the standard setup is the measurement of individual beam intensities; half of the backscatter signal is directly detected using a single photodetector and only half is sent for interference with the LO, whose intensity is measured with a power meter.

Our experimental setup is depicted in Fig. 1. Light from a narrow linewidth laser at 1550 nm is split using a 90:10 splitter into a probe and LO branch, respectively. The probe branch is modulated into 100-ns duration pulses at 20-kHz repetition rate by an acousto-optic modulator (AOM) that also provides a 110-MHz frequency upshift to the beam. This probe signal is then amplified using a pulsed EDFA and sent to a 4.4-km fiber-under-test (FUT) using the transmission port of a three-port circulator. The circulator collects the backscattered signal (BSS) via its reflected port and sends it to an EDFA preamplifier. In a standard ϕ-OTDR setup based on coherent heterodyne detection [12], at this point, the BSS is interfered in a 2×2 50:50 coupler with the LO. However, in our approach, we first split the BSS using a 1×2 50:50 coupler; half of this light is sent to a 2×2 50:50 coupler, as in the standard case, while the other half is sent for direct detection by a single photodetector, thus giving us S_0'. As for the intensity of the LO, S_0'', it remains constant and can be measured one time using a power meter. The interference of LO with S_0' takes place in the 2×2 50:50 coupler. Its output is fed to a balanced photodetector that downshifts the frequency to 110 MHz, thereby providing the beat signal, S_0. Outputs of both photodetectors are sampled at 250 MS/s each via a high-speed data acquisition system. The N in Eq. (1) translates to the number of samples in each beat period. Here, $N = 2$ because the 110-MHz beat signal, sampled at 250 MS/s, gives 2.27 samples for each period.

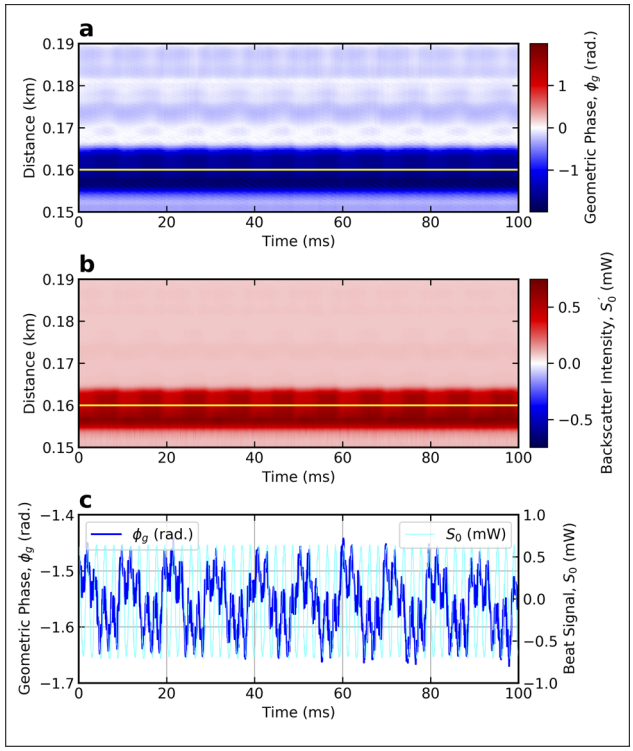

Fig. 2. Inline polarization scrambler (PSM) located at 0.16 km of the fiber-under-test, marked by the horizontal yellow line in the distance–time contour plot of: (a) geometric phase ϕ_g; (b) backscatter intensity, S_0'; (c) geometric phase ϕ_g (blue, left) and backscatter intensity S_0' (cyan, right) versus time at 0.16 km.

Results and discussion. The geometric phase changes with a change in either the SOP or the intensity of one of the interfering beams [9]. The setup shown in Fig. 1 is used to see the effect of varying both the SOP and the intensity of the probe signal by using a polarization scrambler (PSM) and a piezoelectric transducer (PZT) in the FUT, respectively. The distance–time plots of the geometric phase, its power spectral density (PSD), and behavior of $|\gamma_0|$ for both cases are discussed below.

For the first test scenario, a 160-m-long patch cable coming from the transmission port of the three-port circulator, connects an inline polarization scrambler to the 4.4-km fiber-under-test (FUT). A PSM modulates the SOP of the probe signal in the FUT in response to a 100-Hz sinosoidal signal provided by a signal generator for 0.5 s. Distance–time contour plots of the geometric phase, ϕ_g, and the corresponding backscatter intensity, S_0', are plotted in Figs. 2(a) and 2(b), respectively. Figure 2(a) shows that ϕ_g indeed corresponds to the test signal in frequency and amplitude, implying that SOP modulation caused by the PSM is reflected in ϕ_g. It is observed in Fig. 2(b) that the SOP modulation of the probe signal also affects the intensity of backscatter, S_0'. Thus, we are not able to see the impact of only the SOP changing without a corresponding change in the intensity of light. Nonetheless, ϕ_g is not a direct function of S_0' as seen clearly at the end of the fiber at approximately 4.5 km, shown in Fig. 3 where ϕ_g and S_0' are plotted on the left and right axis, respectively. Thus, the modulation of ϕ_g carried forward along

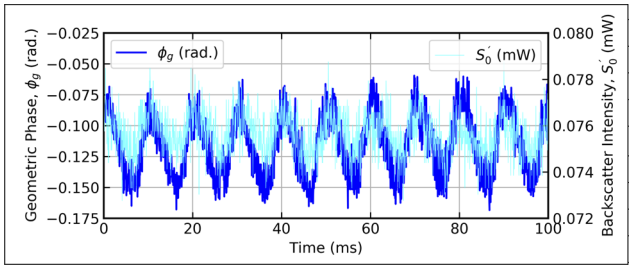

Fig. 3. Geometric phase ϕ_g (blue, left) and backscatter intensity S_0' (cyan, right) near the end of the fiber-under-test at 4.5 km.

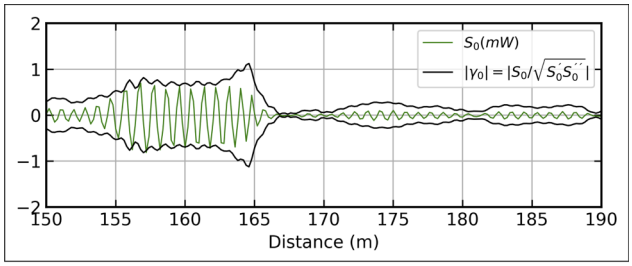

Fig. 4. Beat signal S_0 in mW (green) and normalized envelope signal $|\gamma_0|$ (black) versus distance for the case of an inline polarization scrambler (PSM) at a fiber distance of 0.16 km.

the length of the fiber with higher fidelity to the test signal, as compared to S_0', can be attributed to the change in SOP, independent of the change in intensity, of the backscatter signal. The above mentioned trend of ϕ_g can be observed more clearly in its time series plot given in Fig. 2(c) on the left axis at the location of the PSM at 0.16 km [marked by a horizontal yellow line in Figs. 2(a) and 2(b)]. On the right axis, S_0 is plotted overlapping with ϕ_g to show that the frequency of S_0 along the time axis corresponds to the high-frequency components in ϕ_g. Now, we look at the plot of $|\gamma_0|$ in Fig. 4, which is an important variable in Eq. (1), reflective of the beat signal, S_0, obtained from coherent heterodyning of S_0' with the LO, overlapped with S_0 itself along the distance axis. Here, $|\gamma_0|$ varies with the beat signal amplitude but does not closely follow it especially around the location of the PSM at 164 m. In the standard ϕ-OTDR based on coherent heterodyne [12], the envelope of S_0 effectively reconstructs the backscatter intensity. Thus, the deviation of $|\gamma_0|$ from $|S_0|$ may signal the effect of the change in SOP of the probe signal, independent of its intensity. Figure 5 shows the PSD of ϕ_g, S_0, and S_0' at 0.16 km. The frequency component of the applied acoustic signal at 100 Hz as well as its higher-order harmonics are seen in PSDs of both S_0' and ϕ_g. The aliasing in the PSD of ϕ_g here is attributable to the small N and may be improved by having more samples in each beat period. This is possible by increasing the sampling rate or frequency-offset of the AOM. In addition, S_0 shows modulation along the time axis at approximately 500 Hz – an alias of the pulse repetition frequency of 20 kHz which is also the sampling frequency along the time axis – discussed before in the time domain in Fig. 2(c). In fact, the PSD of ϕ_g in Fig. 5 also contains the second harmonic at approximately 1 kHz which is not seen in the PSD of S_0 itself. Thus, the experiment with PSM shows that the geometric phase is indeed modulated by the SOP of the probe signal, independent of a corresponding change in S_0'.

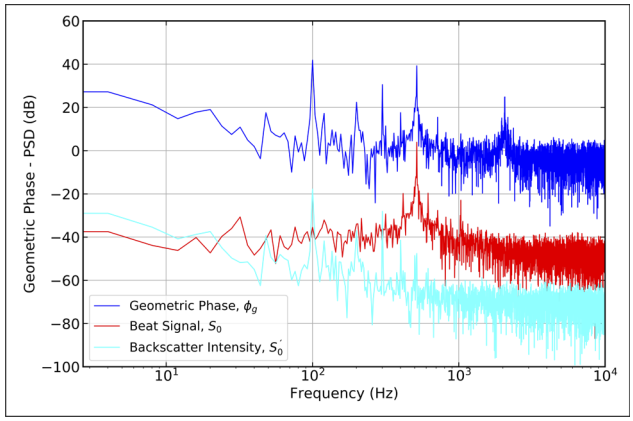

Fig. 5. Power spectral density (PSD) of the geometric phase, ϕ_g, beat signal, S_0, and backscatter intensity, S_0', for an inline polarization scrambler (PSM) at 0.16 km of the fiber-under-test.

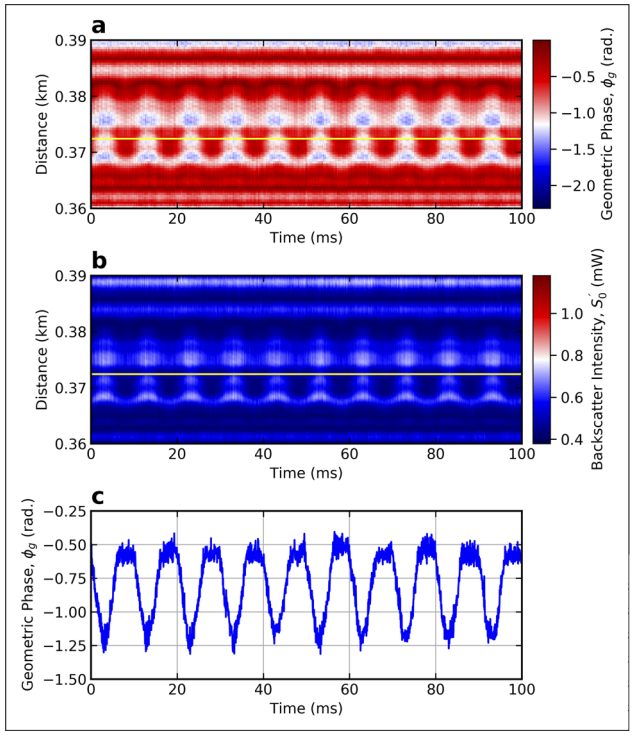

Fig. 6. Inline piezoelectric transducer (PZT) located at 0.373 km of the fiber-under-test, marked by a horizontal yellow line in the distance–time contour plot of: (a) geometric phase ϕ_g; (b) backscattered intensity S_0'; (c) geometric phase ϕ_g (left) and backscattered intensity S_0' (right) versus time at 0.373 km.

In the second test scenario, approximately 375 m into the 4.4-km FUT, 15 m of fiber is wound around a cylindrical PZT. The PZT diameter expands in proportion to the applied voltage causing the fiber section wound around it to experience strain. The strain affects the intensity and phase of the backscatter signal corresponding to the test signal applied to the PZT by the signal generator at 100 Hz for 0.5 seconds. Distance–time contour plots of the geometric phase, ϕ_g, and the corresponding backscatter intensity, S_0', are plotted in Figs. 6(a) and 6(b), respectively. It is observed in Fig. 6(a) that ϕ_g indeed behaves correspondingly to

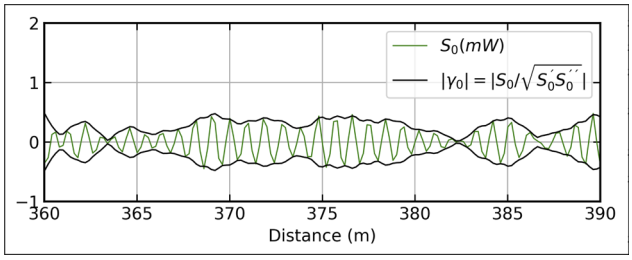

Fig. 7. Beat signal, S_0 (mW), and normalized envelope signal, $|\gamma_0|$, versus distance for inline piezoelectric transducer (PZT) at 0.373 km of the fiber-under-test.

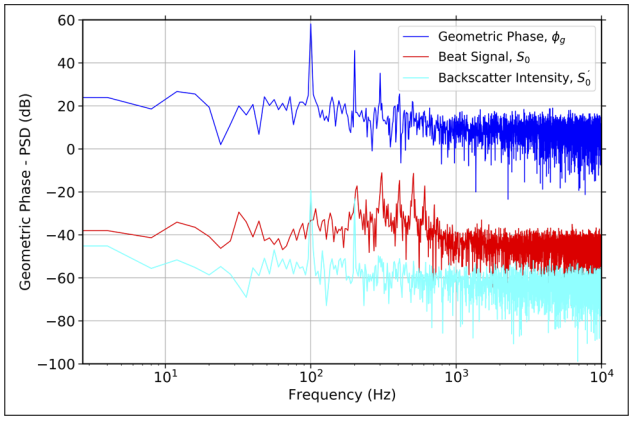

Fig. 8. Power spectral density (PSD) of the geometric phase, ϕ_g, beat signal, S_0, and backscattered intensity, S_0', for inline piezoelectric transducer (PZT) at 0.373 km of the fiber-under-test.

a test signal, implying that the phase and intensity modulation caused by the PZT is reflected by ϕ_g. Figure 6(b) shows that S_0' is also modulated by the strain caused by the PZT to the probe branch. Time series of ϕ_g around the location of the PZT at 0.373 km, marked by a horizontal yellow line in Figs. 6(a) and 6(b), is plotted in Fig. 6(c). In this case, the relative SOP of the two interfering beams, S_0' and S_0'', is relatively constant (this being the underlying assumption/condition for coherent heterodyne detection), so we can observe the effect of a change in intensity only on ϕ_g. In Fig. 7, $|\gamma_0|$, which is the normalized amplitude of S_0 as per Eq. (2), is plotted against S_0 itself. In contrast to Fig. 4, the envelope closely follows S_0. This behavior is similar to the standard coherent heterodyne [12], as mentioned already in the discussion on Fig. 4. This further strengthens the assumption that given the relatively stable SOP of the probe signal with respect to LO, ϕ_g is affected by S_0' only. Figure 8 shows the power spectral density of ϕ_g, S_0, and S_0' at 0.373 km. As in the case with the PSM, the test signal frequency of 100 Hz can be seen in both ϕ_g and S_0' along with higher order harmonics. In this case also, the PSD of S_0 shows frequency modulation at approximately 500 Hz along the time axis, an alias of the 20-kHz sampling frequency along the time axis. However, in this case S_0 is itself modulated by S_0', as shown by peaks at 200 Hz and the following harmonics (the test signal frequency of 100 Hz is not seen, possible due to relatively small sampling rate of 250 MS/s of the 110-MHz beat signal). This is in contrast to the first test scenario with PSM, where S_0 has a single-frequency component at approximately 500 Hz. Thus, with a PZT in the FUT, we have demonstrated that the geometric phase is indeed influenced by a change in intensity of S_0' when the SOP of the interfering beams is relatively constant.

In conclusion, we have measured the geometric phase using a novel phase-sensitive optical time-domain reflectometer setup based on simultaneous direct detection and coherent heterodyne detection. By testing the setup with a polarization scrambler and a piezoelectric transducer in the fiber-under-test, we have shown that the geometric phase is affected by both a change in polarization state and in intensity of the backscatter signal with respect to the constant local oscillator, as anticipated [9]. To our knowledge, this is the first measurement of the geometric phase in the time domain in an optical fiber medium as well as the first with varying beam intensities. Thus, the results are important for characterizing the behavior of the geometric phase as applied to distributed fiber sensing. Further research will be directed toward developing sensing technology based on these results and its evaluation in comparison with the current state-of-the-art. The results should also be applicable to optical communication.

Funding. Bundesanstalt für Materialforschung und 238 -Prüfung (BAM).

Acknowledgments. The authors are grateful to S. Münzenberger for technical support. S.S. acknowledges useful discussions with A. Hannonen.

Disclosures. The authors declare no conflicts of interest.

Data availability. Data underlying the results presented in this paper are available on request.

REFERENCES

1. S. Pancharatnam, Proc. Indian Acad. Sci. **44**, 398 (1956).
2. A. Tomita and R. Y. Chiao, Phys. Rev. Lett. **57**, 937 (1986).
3. M. Martinelli and P. Vavassori, Opt. Commun. **80**, 166 (1990).
4. J. Ferrari, E. Frins, and W. Dultz, J. Lightwave Technol. **15**, 968 (1997).
5. M. G. Kuzyk, J. Opt. Soc. Am. B **19**, 2346 (2002).
6. F. Wassmann and A. Ankiewicz, Appl. Opt. **37**, 3902 (1998).
7. A. Hannonen, H. Partanen, J. Tervo, T. Setälä, and A. T. Friberg, Phys. Rev. A **99**, 053826 (2019).
8. A. Hannonen, H. Partanen, A. Leinonen, J. Heikkinen, T. K. Hakala, A. T. Friberg, and T. Setälä, Optica **7**, 1435 (2020).
9. A. Hannonen, K. Saastamoinen, L.-P. Leppänen, M. Koivurova, A. Shevchenko, A. T. Friberg, and T. Setälä, New J. Phys. **21**, 083030 (2019).
10. Y. Rao, Z. Wang, H. Wu, Z. Ran, and B. Han, Photonic Sens. **11**, 1 (2021).
11. O. E. DeLange, IEEE Spectrum **5**, 77 (1968).
12. Y. Lu, T. Zhu, L. Chen, and X. Bao, J. Lightwave Technol. **28**, 3243 (2010).
13. M. Ren, P. Lu, L. Chen, and X. Bao, IEEE Photonics Technol. Lett. **28**, 697 (2016).
14. Z. He and Q. Liu, J. Lightwave Technol. **39**, 3671 (2021).